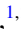




## Robust retrieval method of crystal transition dipole moments by high-order harmonic spectrum

Yue Qiao <sup>1,2,3</sup>, Yanqiu Huo,<sup>1</sup> Huaqiu Liang,<sup>1</sup> Jigen Chen <sup>1,\*</sup>, Wenjun Liu,<sup>4,†</sup> Yujun Yang,<sup>2,3,‡</sup> and Shicheng Jiang <sup>5,§</sup>

<sup>1</sup>Zhejiang Provincial Key Laboratory for Cutting Tools, Taizhou University, Jiaojiang 318000, Zhejiang, China

<sup>2</sup>Institute of Atomic and Molecular Physics, Jilin University, Changchun 130012, China

<sup>3</sup>Jilin Provincial Key Laboratory of Applied Atomic and Molecular Spectroscopy (Jilin University), Changchun 130012, China

<sup>4</sup>State Key Laboratory of Information Photonics and Optical Communications, School of Science, P. O. Box 91, Beijing University of Posts and Telecommunications, Beijing 100876, China

<sup>5</sup>State Key Laboratory of Precision Spectroscopy, East China Normal University, Shanghai 200062, China



(Received 17 August 2022; revised 15 January 2023; accepted 23 January 2023; published 6 February 2023)

According to the three-step model for solid high-order harmonic generation, there is a one-to-one correspondence between the emitted photon energy and the band gap where the electron-hole pair is annihilated. In the tunneling excitation regime, as the electron-hole pair is mostly created in the vicinity of the minimum band gap, the conversion efficiency of the high-energy photon should be approximately proportional to the square of the transition dipole moment at the  $\mathbf{k}$  point where the high-harmonic photon is emitted. Based on this picture we propose that a high-order harmonic spectrum could be a strong tool to reconstruct the shape of  $\mathbf{k}$ -dependent transition dipole moments with the band dispersion and the laser field known. Two real systems, e.g., MgO and ZnO, are taken as samples to verify our idea. The reconstructed shape of the transition dipole moments shows small variation as the laser parameters, such as intensity, wavelength, and pulse duration, are tuned in wide ranges, which proves this scheme is robust.

DOI: [10.1103/PhysRevB.107.075201](https://doi.org/10.1103/PhysRevB.107.075201)

### I. INTRODUCTION

To characterize the structure of solid samples in real space, many techniques, such as electron diffraction, x-ray diffraction, STM, etc. have been developed [1,2]. Crystal with a periodic arrangement of atoms can also be described by band theory in phase space. The chemical and optical properties of the crystal can be well interpreted by band dispersions and transition dipole moments (TDM) between bands. So, in the past decades, researchers have promoted the angle-resolved photon electron spectrum technique greatly to achieve both static and time-resolved reconstruction of occupied bands [3–5]. The optical spectrum is an alternative tool to retrieve the band structure information of the crystal. Especially as the crystal is radiated by strong femtosecond lasers, the excited electrons can be driven to reach the edge of the first Brillouin zone and high-energy photons can be emitted due to electron-hole pair recolliding [6–8]. Since the accumulated phase of the electron (hole) wave packet during the acceleration is encoded in the emitted photon, bands and Berry curvature can be obtained by a decoding step. Both high-order harmonic generation (HHG) and high-order sideband generation have been applied to retrieve the band dispersion and Berry cur-

vature successfully, based on this recolliding physical picture [9–15].

As another basic element in band theory, transition dipole moments between bands also play crucial roles in determining crystal properties. While approaches to retrieve the structure of transition dipole moments were rarely reported. In Ref. [16], Uchida and coauthors visualized the texture of the TDM based on the polarization states of the HHG. In Refs. [17,18], it was reported that a minimum in the  $\mathbf{k}$ -dependent TDM leads to a corresponding minimum deep in the HHG spectrum, which is analogous to the Cooper minimum in the gaseous HHG or the photon-electron spectrum. This phenomenon triggered us to think about whether we can retrieve the amplitude of the  $\mathbf{k}$ -dependent TDM. Our recent works [19,20] tried to reconstruct the TDM through a continuous harmonic spectrum generated by a single quantum trajectory, which needs single or even half-cycle lasers. The strict requirements make it difficult to be realized in real experiments and widely applied. Recently, by establishing the relation between the TDM and the harmonic yield, Ref. [21] proposed a scheme to reconstruct the TDM by a multicycle laser pulse. As we know, a general retrieval method should be not be sensitive to the laser parameters, otherwise it could be difficult in experiments.

Laser parameter-insensitive retrieval method based on quantitative rescattering (QRS) theory for gaseous targets has been established for a long time [22–24]. Let us briefly introduce the basic idea of QRS theory here. According to QRS theory, HHG amplitude can be expressed as the product of a returning electron wave packet with various electron-ion

\*kiddchen@126.com

†jungliu@bupt.edu.cn

‡yangyj@jlu.edu.cn

§scjiang@lps.ecnu.edu.cn

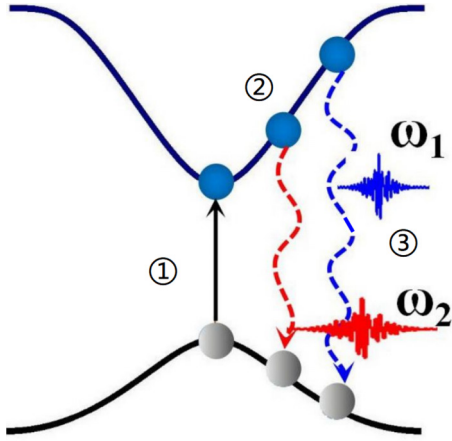


FIG. 1. Schematic illustration of the harmonic generation mechanism for the MgO crystal in the momentum space.

scattering cross sections  $D(\omega) = d(\omega)W(E)$ , where  $W(E)$  is the so-called wave packet mainly determined by the ionization potential of the target,  $d(\omega)$  is the cross section containing the target information. By taking a known atom, with the ionization potential being close to the unknown target, as a reference, the cross section of the unknown target can be obtained by  $|d(\omega)| = |\frac{D(\omega)}{W_{ref}(E)}|$ . Usually, the wave packet of the reference target can be calculated by an accurate time-dependent Schrödinger equation (TDSE) [25]. In principle, this method is insensitive to the driving laser parameters and the retrieval can be finished by a single-shot experiment. The validity and generality had been verified in many previous works [26–28].

## II. QUANTITATIVE RESCATTERING MODEL OF SOLIDS

The success of QRS model for the gaseous medium also provides an opportunity to reconstruct structure information of crystal targets [29]. In the following, we will show how to extend the QRS model from the gaseous target to the crystal. Analogous to HHG from the gaseous medium, solid-HHG can be described by a three-step model [30], e.g., producing a electron-hole pair by excitation, acceleration of the electron (hole) on the conduction (valence) band, and finally a photon emission by the electron-hole recombination. The three-step process is briefly depicted in Fig. 1.

By single-particle and strong-field approximations, the complex spectrum generated by the three-step process reads [31] (atomic units are used throughout this paper unless otherwise stated):

$$D(\omega) = \int_{BZ} dk d(\mathbf{k}) \int_{-\infty}^{\infty} dt e^{-i\omega t} \int_{-\infty}^t dt' F(t') d^*(\boldsymbol{\kappa}_{t'}) \times e^{-iS(\mathbf{k}, t', t)} + \text{c.c.} \quad (1)$$

where the action  $S(\mathbf{k}, t', t) = \int_{t'}^t \varepsilon_g(\boldsymbol{\kappa}_\tau) d\tau$ ,  $\boldsymbol{\kappa}_\tau = \mathbf{k} - \mathbf{A}(t) + \mathbf{A}(\tau)$  is the momentum value where the electron-hole pair is created,  $\mathbf{k}$  is the momentum point where the electron-hole pair is annihilated, and  $\mathbf{A}(t)$  is the vector potential of the incident laser field.  $\varepsilon_g$  represents the band gap between valence and conduction bands.  $F(t) = -\partial_t \mathbf{A}(t) = I_0 f(t) \cos(\omega_0 t)$  is the

laser field with a Gaussian envelope. The threefold integral over  $\mathbf{k}$ ,  $t$ , and  $t'$  can be simplified by the saddle-point approximation [32]. The resulting saddle-point condition for the integral over  $t$  is

$$\frac{dS}{dt} = \varepsilon_g(\mathbf{k}) - \omega = 0. \quad (2)$$

The meaning of the saddle-point solution can be found in Ref. [32]. One key point we want to stress here is that Eq. (2) governs the energy conservation, e.g., the emitted photon energy equals the band gap. According to this classical picture, the spectrum is proportional to

$$D(\omega) \sim d(\omega) \int_{-\infty}^{\infty} dt e^{-i\omega t} \int_{-\infty}^t dt' F(t') d^*(\boldsymbol{\kappa}_{t'}) \times e^{-iS(\mathbf{k}, t', t)} + \text{c.c.}, \quad (3)$$

where the transition dipole moment between valence and conduction bands  $d(\mathbf{k})$  is written in the energy domain  $d(\omega)$ . The frequency  $\omega$  and the momentum  $\mathbf{k}$  satisfy the relationship of  $\omega = \varepsilon(\mathbf{k})$ . In this paper, we only consider the simple case that the transition dipole moments are real numbers. Then Eq. (3) can be recast to

$$D(\omega) \sim d(\omega)W'(\omega), \quad (4)$$

where  $W'(\omega) = \int_{-\infty}^{\infty} dt e^{-i\omega t} \int_{-\infty}^t dt' F(t') d^*(\boldsymbol{\kappa}_{t'}) e^{-iS(\mathbf{k}, t', t)} + \text{c.c.}$  Note that, the  $\mathbf{k}$ -dependent TDM  $d(\boldsymbol{\kappa}_{t'})$  is still contained in the expression of  $W'(\omega)$ . That means the present form of the spectrum is just similar to the gaseous medium case, but can not be used directly to reconstruct the TDM since the TDM information is still entangled in the wave packet.

The saddle-point condition for the integral over  $t'$  is

$$\frac{dS}{dt'} = \varepsilon_g(\mathbf{k} - \mathbf{A}(t) + \mathbf{A}(t')) = 0. \quad (5)$$

This condition determines the birth time of the electron-hole pair in the classical sense. As we know, the minimum band gap should be larger than zero. It means the birth time  $t'$  is a complex number, the imaginary part of which indicates the tunneling behavior. The Keldysh and Zener tunneling rate formula tell us the ionization rate decays exponentially with an increasing band gap. Thus, it is valid to assume that electron-hole pairs of direct band gap semiconductors are mostly created around the minimum band gap.

To verify the validity of our assumption, we present the  $\mathbf{k}$ -dependent electron populations on the conduction band of the MgO crystal in Fig. 2. And in order to see the ionization time more clearly, the time-dependent electronic population of MgO on the conduction band is also given in the figure, which is marked by the solid black line. For different laser parameters, the Keldysh parameters  $\gamma$  in Figs. 2(a)–2(d) are 0.75, 1.96, 0.57, and 1.47, respectively. And  $\gamma$  is the well-known parameter describing the ionization mechanism [33,34]. It can be seen from Figs. 2(a)–2(d) that, for different  $\gamma$ , the excitation of electrons is concentrated around  $\mathbf{k} = \mathbf{0}$ . In other words, the generation probability of the electron-hole pair is greatest around the minimum band gap.

It can be known from the above that the electron-hole pair of direct band gap semiconductors are mostly created around the minimum band gap. Thus, we can approximately regard

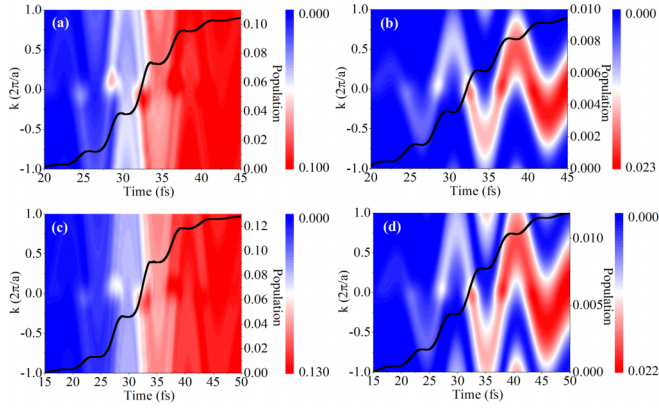


FIG. 2. The time evolution of the electronic density distribution of the MgO crystal at different crystal momenta in the conduction band. The black solid line represents the time-dependent electronic population of the conduction band. Laser parameter: (a) 2400 nm,  $2 \times 10^{13}$  W/cm<sup>2</sup>; (b) 2400 nm,  $3 \times 10^{12}$  W/cm<sup>2</sup>; (c) 3200 nm,  $2 \times 10^{13}$  W/cm<sup>2</sup>; (d) 3200 nm,  $3 \times 10^{12}$  W/cm<sup>2</sup>.

the  $d(\kappa_{t'})$  where the electron-hole pair is created as a constant  $C$ . Then the TDM information  $d(\kappa_{t'})$  entangled in the wave packet can be eliminated. Equation (4) can be written as:

$$D(\omega) \sim d(\omega)W(\omega), \quad (6)$$

where  $W(\omega) = C \int_{-\infty}^{\infty} dt e^{-i\omega t} \int_{-\infty}^t dt' F(t') e^{-iS(\kappa, t', t)} + c.c.$

According to Eq. (6), assuming the laser parameters and the band dispersion are known, we can calculate the reference wave packet  $W_{ref}(\omega)$ , which is similar to the gaseous target. Once the spectra signal  $D(\omega)$  is measured, the TDM can be reconstructed directly by

$$d(\omega) \sim \frac{D(\omega)}{W_{ref}(\omega)}. \quad (7)$$

### III. ALL-OPTICAL RECONSTRUCTION OF TDM BY QRS

In the following, the idea shown above will be applied to reconstruct the TDM of two real systems, e.g., MgO and ZnO, which belong to direct band gap crystals, and we will examine the robustness of our scheme. The HHG spectra calculated by the semiconductor Bloch equations (SBEs) with *ab initio* simulated bands and TDMs as input [35–38] will be regarded as the standard spectra signal  $D(\omega)$ .

In Fig. 3(b), the *ab initio* simulated TDM, which will be referred to as target and the reconstructed TDM are put together for comparison. The real TDM of the MgO in the  $\Gamma$ -X direction [blue solid line in Fig. 3(b)] is obtained by the density functional theory (DFT) package in VASP using the Perdew-Burke-Ernzeroff (PBE) generalized gradient approximation functional. When the  $\mathbf{k}$ -dependent TDM of the MgO is projected into the energy domain, its range is about 7.8 eV–17.2 eV. The corresponding HHG spectrum calculated by the SBEs is presented by the black solid line in Fig. 3(a). The horizontal axis is photon energy and the vertical axis is harmonic intensity. Here, the laser intensity and the center wavelength of the laser field are  $4 \times 10^{12}$  W/cm<sup>2</sup> and 2400 nm. The pulse duration of the driving laser pulse and the dephasing time are 17 fs and 1 fs. The red dotted line

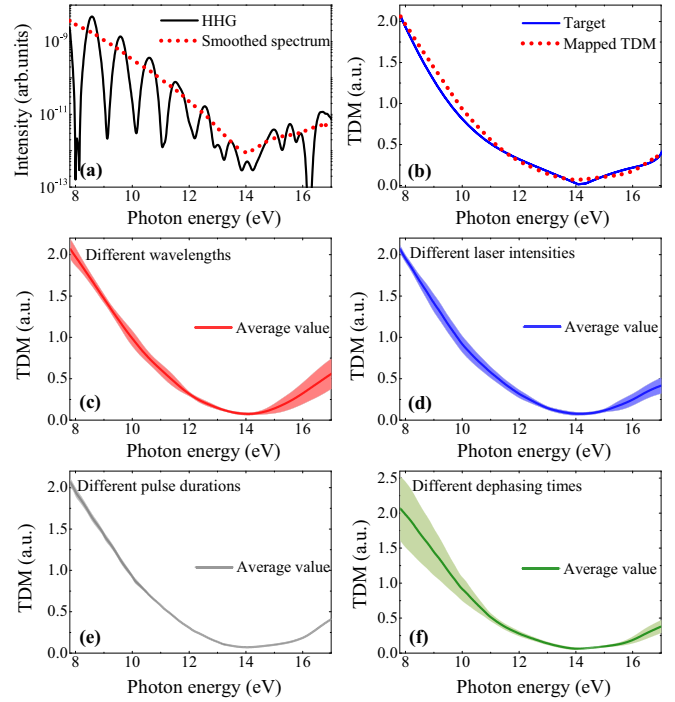


FIG. 3. (a) The harmonic spectrum generated by  $4 \times 10^{12}$  W/cm<sup>2</sup>, 2400 nm, and 17 fs driving laser. The red dotted line is the Gaussian smoothed spectrum. (b) The comparison of the *ab initio* calculated and retrieved TDMs using the smoothed spectrum in (a). A scaling factor is multiplied to set the maximum of the retrieved and *ab initio* calculated TDMs to be the same. The average value and standard deviation of the reconstructed TDM at (c) different wavelengths; (d) different laser intensities; (e) different pulse durations; (f) different dephasing times. We set  $C = 2$  in Eq. (6).

in Fig. 3(a) is the smoothed harmonic spectrum by Gaussian function  $G(x) = \frac{1}{\sqrt{2\pi}\sigma} e^{-\frac{x^2}{2\sigma^2}}$  with  $\sigma = 5\omega_0$ , and  $\omega_0$  is the fundamental frequency of the laser field. Figure 3(b) shows that the shape of the reconstructed TDM agrees well with the target TDM.

In order to demonstrate the robustness of our method, we calculate the average value and the corresponding standard deviation of the reconstructed TDMs under different laser parameters in Figs. 3(c)–3(e). Except for the changed parameters, the other parameters are the same as those in Fig. 3(b). Figure 3(c) depicts the average value of reconstructed TDM when the wavelength changes from 1700–2600 nm with a step size of 100 nm, as shown by the red solid line in the figure. Their standard deviation is filled with the light red. The formulas for average value and standard deviation are  $\bar{X} = \frac{\sum_{i=1}^n X_i}{n}$  and  $s = \sqrt{\frac{\sum_{i=1}^n (X_i - \bar{X})^2}{n-1}}$ , respectively. We can see that the variation range of the standard deviation is very small, which means the difference in the wavelength has less influence on the reconstruction result. Figure 3(d) presents the average value (blue solid line) and the standard deviation (light blue shading) of reconstructed TDMs when  $I_0 = 2 \times 10^{12}$  W/cm<sup>2</sup> –  $6 \times 10^{12}$  W/cm<sup>2</sup> with the step of  $5 \times 10^{11}$  W/cm<sup>2</sup>. Under this condition, the range of the standard deviation is also small, and the shape of the TDM can

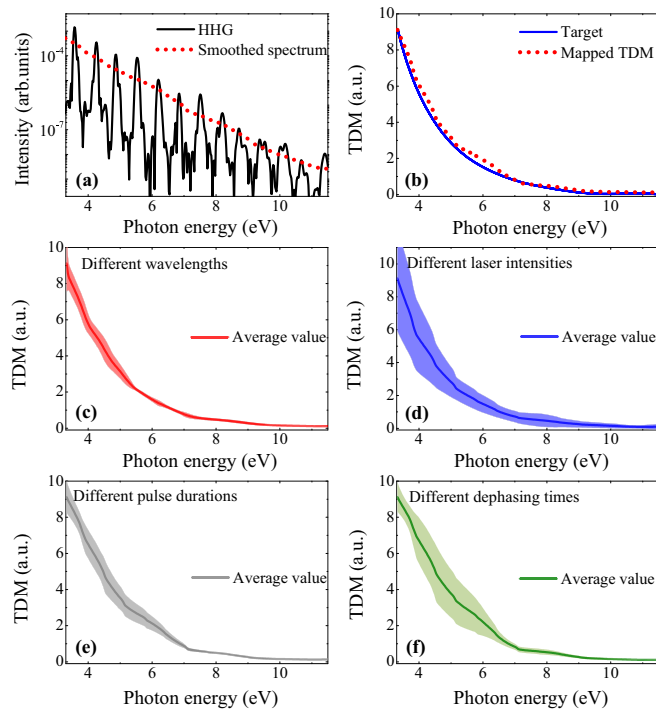


FIG. 4. (a) The harmonic spectrum generated by  $1 \times 10^{12}$  W/cm<sup>2</sup>, 3800 nm, and 60 fs driving laser. The red dotted line is the Gaussian smoothed spectrum. (b) The comparison of the *ab initio* calculated and retrieved TDMs using the smoothed spectrum in (a). A scaling factor is multiplied to set the maximum of the retrieved and *ab initio* calculated TDMs to be the same. The average value and standard deviation of the reconstructed TDM at (c) different wavelengths; (d) different laser intensities; (e) different pulse durations; (f) different dephasing times.

still be reconstructed well. (The reconstructed results under stronger laser intensities can be found in Appendix A.) Figure 3(e) exhibits the average value of retrieved TDM at a pulse duration of 16 fs–48 fs with a step size of 4 fs, as shown by the gray solid line in the figure. The standard deviation is filled with the light gray. It can be seen that the standard deviation of the reconstructed TDM is very small when the laser duration varies from two cycles to six cycles. Our reconstruction scheme can also get better results in the multicycle field. We also examined the effect of the dephasing time of SBEs on the reconstructed results. Figure 3(f) shows the average value of reconstructed TDMs at a dephasing time of 0.5 fs–2 fs and the step is 0.5 fs, as shown by the green solid line in the figure. The standard deviation is filled with the light green. We can observe that the change of the dephasing time also has little influence on the reconstructed TDM. Overall, our reconstruction scheme is less dependent on laser parameters and the dephasing time. In most conditions, the reconstructed results of TDM are in good agreement with the target TDM.

To demonstrate the universality of our retrieved scheme, we also detect the TDM from the harmonic spectrum of the ZnO crystal. Figure 4(b) gives the TDM of the ZnO crystal along the  $\Gamma$ - $M$  direction (blue solid line), which is also obtained by the Perdew-Burke-Ernzeroff (PBE) generalize gradient approximation functional in VASP. When the

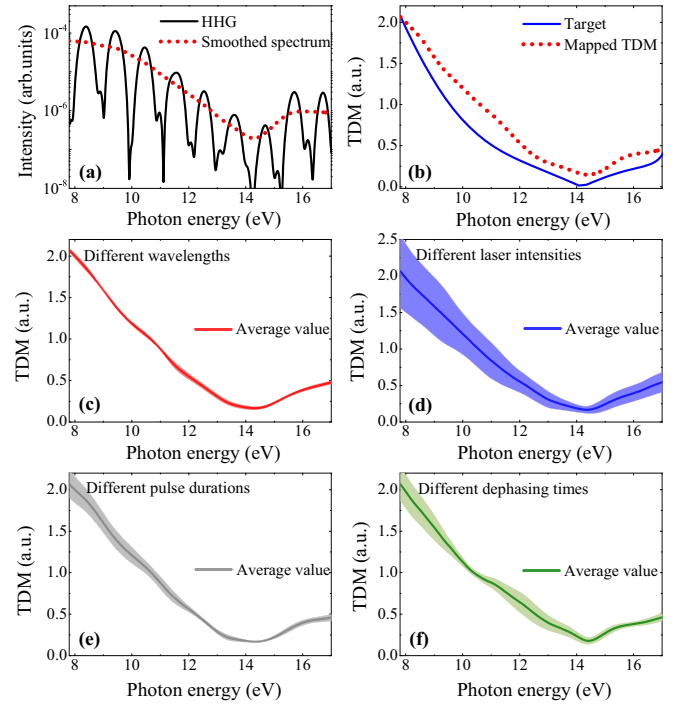


FIG. 5. (a) The HHG spectrum of MgO and the Gaussian smoothed spectrum when laser intensity is  $2 \times 10^{13}$  W/cm<sup>2</sup>. (b) The real TDM and the reconstructed TDM of the MgO crystal. A scaling factor is multiplied to set the maximum of the retrieved and *ab initio* calculated TDMs to be the same. The average value and standard deviation of the reconstructed TDM at (c) different wavelengths; (d) different laser intensities; (e) different pulse durations; (f) different dephasing times.

**k**-dependent TDM of the ZnO is projected into the energy domain, its range is about 3.3 eV–11.5 eV. The reconstructed TDM is presented by the red dotted line in Fig. 4(b). The corresponding HHG spectrum and the Gaussian smoothed spectrum of ZnO are depicted by the black solid line and the red dotted line in Fig. 4(a), respectively. Here, the laser intensity and the center wavelength of the laser field are  $1 \times 10^{12}$  W/cm<sup>2</sup> and 3800 nm. The pulse duration of the laser pulse and the dephasing time are 60 fs and 1.5 fs. One can find from Fig. 4(b) that the shape of the mapped TDM is in good agreement with the real TDM. Similarly, we checked the effect of different laser parameters on the reconstruction results. The solid line and the light area in Figs. 4(c)–4(e) represent the average value and the standard deviation of retrieved TDMs from the HHG spectra with different laser parameters, respectively. Figure 4(c) displays the reconstructed TDMs when the wavelength changes from 3500 nm–4000 nm with a step size of 50 nm. Figure 4(d) shows the mapped results when  $I_0 = 3 \times 10^{11}$  W/cm<sup>2</sup>– $3 \times 10^{12}$  W/cm<sup>2</sup> with the step of  $3 \times 10^{11}$  W/cm<sup>2</sup>. Figure 4(e) presents the retrieved results at a pulse duration of 31 fs–76 fs with a step size of 6 fs. Overall, the change of laser parameters has little effect on the reconstructed TDMs. Figure 4(f) exhibits the mapped results at the dephasing times from 1 fs–3 fs with the step 0.5 fs. It should be noted that according to the Ref. [39], the HHG of ZnO is more sensitive to the dephasing time, so our reconstructed result is more dependent on the dephasing time.

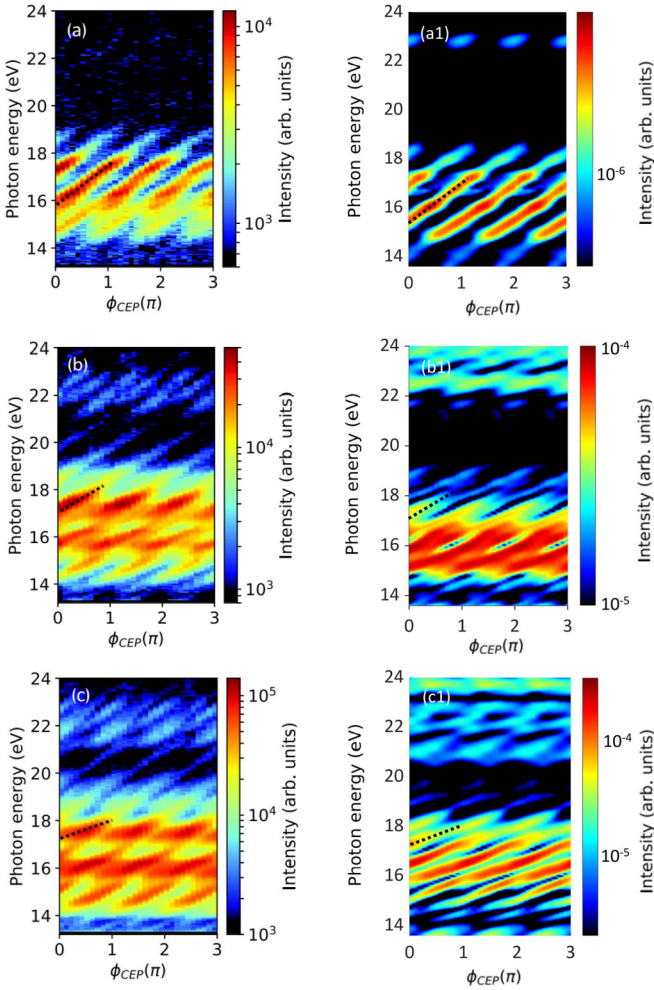


FIG. 6. The CEP dependence of the MgO crystal harmonic spectra from (a)–(c) experimental measure and (a1)–(c1) simulated results. Laser wavelength is 1700 nm with pulse duration of 12 fs. The laser intensity used in (a1) is  $1.91 \times 10^{13}$  W/cm<sup>2</sup>; in (b1) is  $3.84 \times 10^{13}$  W/cm<sup>2</sup>; and in (c1) is  $5.85 \times 10^{13}$  W/cm<sup>2</sup>. (a)–(c) are reprinted with permission from Ref. [42] © The Optical Society.

In terms of above analyses, we can conclude that it is also feasible to image the  $\mathbf{k}$ -dependent TDM of other direct band gap crystals by using this scheme.

#### IV. CONCLUSION

In summary, we have identified the QRS model can be extended from the gaseous target to the solid. With the help of QRS theory for solid-HHG, the TDMs of two direct band gap crystals have been successfully retrieved. By changing the laser parameters in a wide range, we have demonstrated that the reconstruction scheme is robust. This retrieval method can realize a single-shot measurement scheme, and it is easy to operate in the experiment. However, there are some limitations for our proposal. First, all the extended QRS formula for solid-HHG only consider interband components. If the crystal harmonic spectrum is dominated by the intraband current, this scheme can not work well. Second, when the intensity of the incident laser pulse is too strong, Stark shift of energy bands

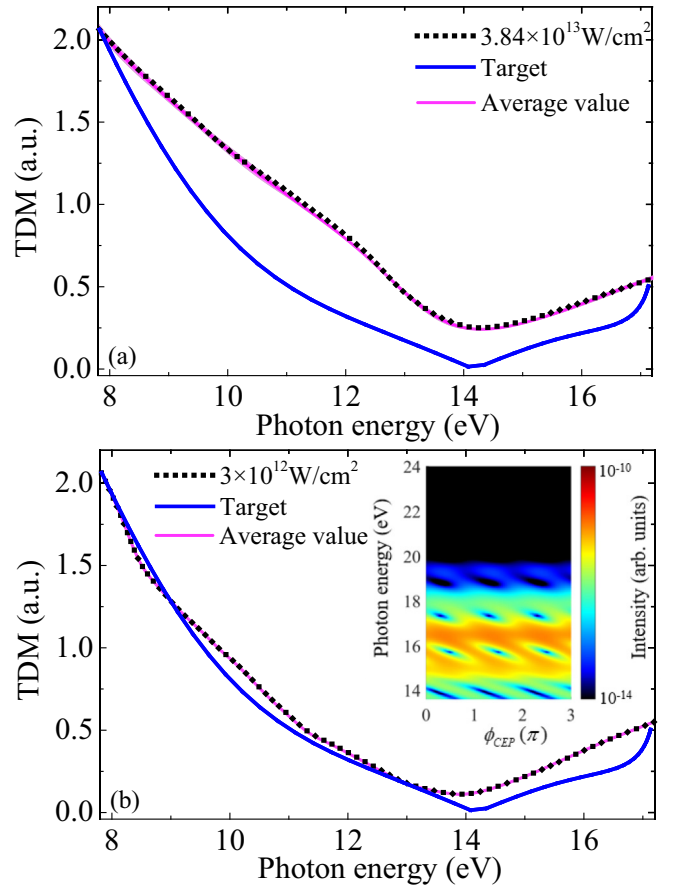


FIG. 7. (a) The retrieved TDM (black dotted line) when the laser intensity is  $3.84 \times 10^{13}$  W/cm<sup>2</sup> and CEP = 0. (b) The retrieved TDM (black dotted line) when the laser intensity is  $3 \times 10^{12}$  W/cm<sup>2</sup> and CEP = 0. The blue line is the *ab initio* calculated TDMs. A scaling factor is multiplied to set the maximum of the retrieved and *ab initio* calculated TDMs to be the same. The average value and standard deviation of the reconstructed TDM at different CEP settings are shown as pink line and light pink shading. The inset of (b) is the CEP dependence of the MgO crystal harmonic spectra under  $3 \times 10^{12}$  W/cm<sup>2</sup>. Laser wavelength is 1700 nm with pulse duration of 12 fs.

may destroy the correspondence of the emitted photon energy and the field-free band structure, and solid-SFA model can not work very well either. Third, it is assumed that electrons are excited around the minimum band gap, and the shape of the  $\mathbf{k}$ -dependent TDM around there is set to be constant in our method. Thus, if this assumption is not valid anymore, the retrieved results should be unreliable. In the case of the large off-resonant excitation, renormalization of band energy and Rabi frequency can be ignored, because the real excitation probability is small [40,41]. Once the excitation probability is high enough, the quantity of band renormalization can reach a few hundred meV [41], then the shape of the HHG spectrum would be tuned, which will influence the accuracy of the reconstructed TDMs. Overall, our work is an important supplement to the all-optical reconstruction method, and it will strongly promote the further development of high-order harmonic detection technology.

## ACKNOWLEDGMENTS

This work was supported by the National Natural Science Foundation of China (Grants No. 11975012, No. 11627807, No. 11774129, and No. 12074145); The National Key Research and Development Program of China (Grant No. 2019YFA0307700); The Outstanding Youth Project of Taizhou University (Grant No. 2019JQ002); The Zhejiang Provincial Natural Science Foundation of China (Grant No. Y23A040001); The Jilin Provincial Research Foundation for Basic Research, China (20220101003JC). S.J. acknowledges the support by the start-up funding from East China Normal University. Y.Q. and Y.Y. acknowledge the High Performance Computing Center of Jilin University for supercomputer time. J.C. and S.J. thank Chii-Dong Lin from Kansas State University for fruitful discussion.

## APPENDIX A: RESULTS USING STRONGER LASER INTENSITY

In fact, we also investigate the variation of the reconstruction results from MgO with laser parameters under much stronger laser intensity. The corresponding HHG spectrum is presented by the black solid line in Fig. 5(a). Here, the laser intensity and the center wavelength of the laser field are  $2 \times 10^{13}$  W/cm<sup>2</sup> and 2400 nm. The pulse duration of the driving laser pulse and the dephasing time are 17 fs and 1 fs. Figure 5(b) shows that although the shape of the reconstructed TDM is similar to the target, it is not as good as the result of the low laser intensity [Fig. 3(b)]. The average value and the corresponding standard deviation of the reconstructed TDM under different laser parameters are also given in Figs. 5(c)–5(e). Except for the changed parameters, other parameters are the same as those in Fig. 5(b). Figure 5(c) depicts the average value of reconstructed TDMs when the wavelength changes from 2200 nm–2600 nm with a step size of 50 nm, as shown by the red solid line in the figure. Their standard deviation is filled with the light red. Figure 5(d) presents the average value and the standard deviation of reconstructed TDMs when  $I_0 = 4 \times 10^{12}$  W/cm<sup>2</sup>– $4 \times 10^{13}$  W/cm<sup>2</sup>, the step is  $4 \times 10^{12}$  W/cm<sup>2</sup>, as shown by the blue solid line and light blue area, respectively. Figure 5(e) exhibits the average value of reconstructed TDMs at a pulse duration of 16 fs–48 fs with a step size of 4 fs, as shown by the gray solid line in the figure. The standard deviation is filled with the light gray. Figure 5(f) shows the average value of reconstructed TDM at a dephasing time of 1 fs–5 fs and the step is 0.5 fs, as shown by the green solid line in the figure. The standard deviation

is filled with the light green. We can see the difference in the wavelength, the pulse duration, and the dephasing time has less influence on the reconstruction result. But when the laser intensity changes by an order of magnitude, the range of the standard deviation will be relatively larger. So, when the laser intensity is too strong, Stark shift of energy bands may destroy the correspondence of the emitted photon energy and the field-free band structure, our model can not work very well.

## APPENDIX B: CEP INFLUENCE ON THE RECONSTRUCTION RESULTS

We examine the influence of the carrier-envelope phase (CEP) on the HHG spectra from the MgO crystal, as shown in Figs. 6(a1)–6(c1). Here, the dephasing time is 0.8 fs, and laser parameters of the incident pulse are 12 fs in pulse duration, 1700 nm in wavelength. The laser intensity of Figs. 6(a1)–6(c1) are  $1.91 \times 10^{13}$  W/cm<sup>2</sup>,  $3.84 \times 10^{13}$  W/cm<sup>2</sup>, and  $5.85 \times 10^{13}$  W/cm<sup>2</sup>, respectively. They are the same as that used in the experiment by You *et al.* [42]. They experimentally measured the dependence of the MgO harmonic frequencies on the CEP of the driving laser pulse, as presented by Figs. 6(a)–6(c). It can be observed that our simulation well reproduces the experimental results: the harmonic spectra apparently exist in the double plateau structure; when the CEP is increased, the harmonic peaks shift toward higher photon energy, forming a slope of photon energy versus the CEP. Furthermore, the CEP slope is nearly consistent with the experimental data. Then the calculated HHG spectrum from CEP = 0 under  $3.84 \times 10^{13}$  W/cm<sup>2</sup> is adopted to retrieve TDM, and the result is displayed in Fig. 7(a). As we previously speculated, when the laser intensity is too strong, our scheme may not work well. The results of Fig. 7(a) further verify our guess. One can notice that the reconstructed result under  $3.84 \times 10^{13}$  W/cm<sup>2</sup> is not good. So in Fig. 7(b), we calculate the result at lower laser intensity  $3 \times 10^{12}$  W/cm<sup>2</sup>, and the other parameters are the same as the Figs. 6(a1)–6(c1). At the same time, the calculated HHG spectra from CEP = 0 under  $3 \times 10^{12}$  W/cm<sup>2</sup> is adopted to retrieve TDM, and the result is displayed in Fig. 7(b). One can see that the mapped TDM (black dashed line) at lower laser intensity agrees better with the real TDM (blue solid line) than the mapped TDM at stronger laser intensity. The inset of Fig. 7(b) shows the effect of the CEP on the crystal harmonic spectra under  $3 \times 10^{12}$  W/cm<sup>2</sup>. We also study the CEP influence on the reconstructed results. From the figure, the standard deviation of the retrieved TDM under different CEP settings is very small and almost invisible, it can be demonstrated that CEP has little effect on the reconstructed results.

[1] A. Winkelmann and G. Nolze, *Ultramicroscopy* **149**, 58 (2015).  
 [2] I. Sychugov, H. Omi, T. Murashita, and Y. Kobayashi, *Nanotechnol.* **20**, 145706 (2009).  
 [3] A. Damascelli, Z. Hussain, and Z.-X. Shen, *Rev. Mod. Phys.* **75**, 473 (2003).  
 [4] A. Damascelli, *Phys. Scr.* **T109**, 61 (2004).  
 [5] E. J. Sie, T. Rohwer, C. Lee, and N. Gedik, *Nature Commun.* **10**, 3535 (2019).  
 [6] L. Yue and M. B. Gaarde, *J. Opt. Soc. Am. B* **39**, 535 (2022).

[7] L. Yue and M. B. Gaarde, *Phys. Rev. Lett.* **124**, 153204 (2020).  
 [8] L. Yue and M. B. Gaarde, *Phys. Rev. A* **103**, 063105 (2021).  
 [9] G. Vampa, T. J. Hammond, N. Thiré, B. E. Schmidt, F. Légaré, C. R. McDonald, T. Brabec, D. D. Klug, and P. B. Corkum, *Phys. Rev. Lett.* **115**, 193603 (2015).  
 [10] L. Li, P. Lan, L. He, W. Cao, Q. Zhang, and P. Lu, *Phys. Rev. Lett.* **124**, 157403 (2020).

- [11] A. A. Lanin, E. A. Stepanov, A. B. Fedotov, and A. M. Zheltikov, *Optica* **4**, 516 (2017).
- [12] T.-J. Shao, L.-J. Lü, J.-Q. Liu, and X.-B. Bian, *Phys. Rev. A* **101**, 053421 (2020).
- [13] C. Yu, S.-C. Jiang, T. Wu, G.-L. Yuan, Z.-W. Wang, C. Jin, and R.-F. Lu, *Phys. Rev. B* **98**, 085439 (2018).
- [14] T. T. Luu and H. J. Wörner, *Nature Commun.* **9**, 916 (2018).
- [15] H. B. Banks, Q. Wu, D. C. Valocin, S. Mack, A. C. Gossard, L. Pfeiffer, R.-B. Liu, and M. S. Sherwin, *Phys. Rev. X* **7**, 041042 (2017).
- [16] K. Uchida, V. Pareek, K. Nagai, K. M. Dani, and K. Tanaka, *Phys. Rev. B* **103**, L161406 (2021).
- [17] S. Jiang, C. Yu, J. Chen, Y. Huang, R. Lu, and C. D. Lin, *Phys. Rev. B* **102**, 155201 (2020).
- [18] Y.-T. Zhao, X.-Q. Xu, S.-C. Jiang, X. Zhao, J.-G. Chen, and Y.-J. Yang, *Phys. Rev. A* **101**, 033413 (2020).
- [19] Y.-T. Zhao, S.-Y. Ma, S.-C. Jiang, Y.-J. Yang, X. Zhao, and J.-G. Chen, *Opt. Express* **27**, 34392 (2019).
- [20] Y. Qiao, Y.-Q. Huo, S.-C. Jiang, Y.-J. Yang, and J.-G. Chen, *Opt. Express* **30**, 9971 (2022).
- [21] D. Wu, L. Li, Y. Zhan, T. Huang, H. Cui, J. Li, P. Lan, and P. Lu, *Phys. Rev. A* **105**, 063101 (2022).
- [22] C. D. Lin, A.-T. Le, Z. Chen, T. Morishita, and R. Lucchese, *J. Phys. B: At. Mol. Opt. Phys.* **43**, 122001 (2010).
- [23] A.-T. Le, R. R. Lucchese, S. Tonzani, T. Morishita, and C. D. Lin, *Phys. Rev. A* **80**, 013401 (2009).
- [24] A.-T. Le, H. Wei, C. Jin, and C. D. Lin, *J. Phys. B: At. Mol. Opt. Phys.* **49**, 053001 (2016).
- [25] Y. Qiao, D. Wu, J.-G. Chen, J. Wang, F.-M. Guo, and Y.-J. Yang, *Phys. Rev. A* **100**, 063428 (2019).
- [26] T. Morishita, A.-T. Le, Z.-J. Chen, and C. D. Lin, *Phys. Rev. Lett.* **100**, 013903 (2008).
- [27] A.-T. Le, R. R. Lucchese, M. T. Lee, and C. D. Lin, *Phys. Rev. Lett.* **102**, 203001 (2009).
- [28] J. Xu, C. I. Blaga, A. D. DiChiara, E. Sistrunk, K. Zhang, Z. Chen, A.-T. Le, T. Morishita, C. D. Lin, P. Agostini, and L. F. DiMauro, *Phys. Rev. Lett.* **109**, 233002 (2012).
- [29] V.-H. Hoang and A.-T. Le, *Phys. Rev. A* **102**, 023112 (2020).
- [30] G. Vampa and T. Brabec, *J. Phys. B: At. Mol. Opt. Phys.* **50**, 083001 (2017).
- [31] G. Vampa, C. R. McDonald, G. Orlando, D. D. Klug, P. B. Corkum, and T. Brabec, *Phys. Rev. Lett.* **113**, 073901 (2014).
- [32] G. Vampa, C. R. McDonald, G. Orlando, P. B. Corkum, and T. Brabec, *Phys. Rev. B* **91**, 064302 (2015).
- [33] S. Ghimire, G. Ndabashimiye, A. D. DiChiara, E. Sistrunk, M. I. Stockman, P. Agostini, L. F. DiMauro, and D. A. Reis, *J. Phys. B: At. Mol. Opt. Phys.* **47**, 204030 (2014).
- [34] A. D. DiChiara, S. Ghimire, C. I. Blaga, E. Sistrunk, E. P. Power, A. M. March, T. A. Miller, D. A. Reis, P. Agostini, and L. F. DiMauro, *IEEE J. Sel. Top. Quantum Electron.* **18**, 419 (2012).
- [35] J. Li, X. Zhang, S. Fu, Y. Feng, B. Hu, and H. Du, *Phys. Rev. A* **100**, 043404 (2019).
- [36] S. Jiang, H. Wei, J. Chen, C. Yu, R. Lu, and C. D. Lin, *Phys. Rev. A* **96**, 053850 (2017).
- [37] L. Yue and M. B. Gaarde, *Phys. Rev. A* **101**, 053411 (2020).
- [38] Y.-T. Zhao, S.-C. Jiang, X. Zhao, J.-G. Chen, and Y.-J. Yang, *Opt. Lett.* **45**, 2874 (2020).
- [39] S. Jiang, J. Chen, H. Wei, C. Yu, R. Lu, and C. D. Lin, *Phys. Rev. Lett.* **120**, 253201 (2018).
- [40] S. C. Liebscher, M. K. Hagen, J. Hader, J. V. Moloney, and S. W. Koch, *Phys. Rev. B* **104**, 165201 (2021).
- [41] U. Huttner, M. Kira, and S. W. Koch, *Laser Photon. Rev.* **11**, 1700049 (2017).
- [42] Y. S. You, M. Wu, Y. Yin, A. Chew, X. Ren, S. Gholam-Mirzaei, D. A. Browne, M. Chini, Z. Chang, K. J. Schafer, M. B. Gaarde, and S. Ghimire, *Opt. Lett.* **42**, 1816 (2017).